AIP Journal of Applied Physics

Size dependent bandgap of molecular beam epitaxy grown InN quantum dots measured by scanning tunneling spectroscopy

Mahesh Kumar, Mohana K. Rajpalke, Thirumaleshwara N. Bhat, Basanta Roul, A. T. Kalghatgi et al.

Citation: J. Appl. Phys. 110, 114317 (2011); doi: 10.1063/1.3665639
View online: http://dx.doi.org/10.1063/1.3665639
View Table of Contents: http://jap.aip.org/resource/1/JAPIAU/v110/i11
Published by the AIP Publishing LLC.

Additional information on J. Appl. Phys.

Journal Homepage: http://jap.aip.org/
Journal Information: http://jap.aip.org/about/about_the_journal
Top downloads: http://jap.aip.org/features/most_downloaded
Information for Authors: http://jap.aip.org/authors

ADVERTISEMENT

Instruments for advanced science

contact Hiden Analytical for further details

HIDEN ANALYTICAL

info@hideninc.com
www.HidenAnalytical.com
CLICK to view our product catalogue

Downloaded 19 Sep 2013 to 142.51.1.212. This article is copyrighted as indicated in the abstract. Reuse of AIP content is subject to the terms at: http://jap.aip.org/about/rights_and_permissions

JOURNAL OF APPLIED PHYSICS **110**, 114317 (2011)

Size dependent bandgap of molecular beam epitaxy grown InN quantum dots measured by scanning tunneling spectroscopy

Mahesh Kumar,[1,2] Mohana K. Rajpalke,[1] Thirumaleshwara N. Bhat,[1] Basanta Roul,[1,2] A. T. Kalghatgi,[2] and S. B. Krupanidhi[1,a)]
[1]*Materials Research Centre, Indian Institute of Science, Bangalore-560012, India*
[2]*Central Research Laboratory, Bharat Electronics, Bangalore-560013, India*

(Received 2 February 2011; accepted 7 November 2011; published online 9 December 2011)

InN quantum dots (QDs) were grown on Si (111) by epitaxial Stranski-Krastanow growth mode using plasma-assisted molecular beam epitaxy. Single-crystalline wurtzite structure of InN QDs was verified by the x-ray diffraction and transmission electron microscopy. Scanning tunneling microscopy has been used to probe the structural aspects of QDs. A surface bandgap of InN QDs was estimated from scanning tunneling spectroscopy (STS) *I-V* curves and found that it is strongly dependent on the size of QDs. The observed size-dependent STS bandgap energy shifts with diameter and height were theoretical explained based on an effective mass approximation with finite-depth square-well potential model. © *2011 American Institute of Physics*.
[doi:10.1063/1.3665639]

I. INTRODUCTION

InN is an interesting and potentially important semiconductor material with superior electronic transport properties.[1] Compared to all other group-III nitrides, InN possesses the lowest effective mass, the highest mobility, and the highest saturation velocity.[2] InN is currently receiving much attention, due to its recently observed narrow bandgap E_g of 0.7 eV.[3] Such properties of InN as narrow bandgap, infra-red photoluminescence in the practical important optical communication wavelengths, possibility of generation of THz emission and superior electron transport properties are very promising for numerous applications of this material. Among all III-nitride semiconductors, InN remains one of the least studied materials because of the difficulty in growing high-quality epitaxial film, due to the low dissociation temperature and the extremely high vapor pressure of nitrogen for InN, as compared with those for AlN and GaN.[4] With the rapid progress in epitaxial growth techniques, the nanoscale InN dots with controllable size and density can be grown using molecular beam epitaxy (MBE). InN quantum dots (QDs) are highly interesting owing to nanometer-scale charge carrier confinement in all three spatial dimensions. This gives rise to quantized energy of the QDs and associated applications such as lasers, photodetectors, light emitting diodes and in THz generations. Scanning tunneling microscopy (STM) has been used in many prior studies to probe the structural aspects of QDs and scanning tunneling spectroscopy (STS) measurements describe a bandgap associated with the dots.[5–7] The effective mass approximation (EMA)[8,9] model was employed by many researchers to understand the size dependent bandgap of low-dimensional systems, because of its simplicity. The other treatments that are used to account for the bandgap of nanoparticles include the effective bond orbital model,[10,11] the tight binding approach,[12,13] empirical pseudopotential method,[14,15] Wannier function method,[16] and density functional theory (DFT).[17] We have studied the STM and STS measurements of individual InN QDs grown on Si (111) substrate. A surface bandgap of InN QDs was estimated from STS *I-V* curves and found that it is strongly dependent on the size of QDs. An EMA with finite-depth square-well potential is used to investigate the size-dependent bandgap of InN QDs.

II. EXPERIMENTAL PROCEDURES

InN dots were grown in an ultrahigh vacuum (UHV) MBE-SPM system (Omicron Nanotechnology), which consists of two UHV chambers (surface probe microscopy (SPM) and MBE) with base pressures better than 1×10^{-10} mbar and an additional high vacuum load-lock chamber. The MBE chamber is equipped with a *K*-cell for indium and an rf plasma source for activated nitrogen. The undoped Si (111) substrate were chemically cleaned followed by dipping in 5% HF to remove the surface oxide and loaded into the MBE

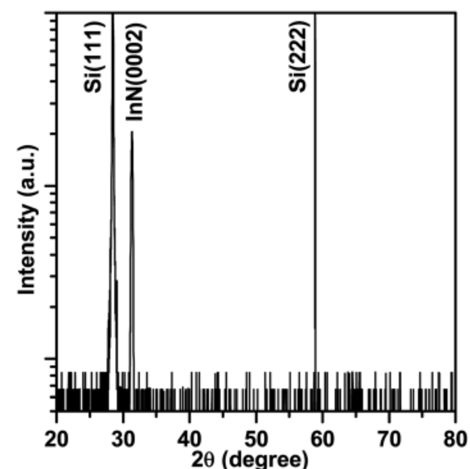

FIG. 1. XRD 2θ-ω pattern of the InN QDs grown on Si (111) substrate, indicating the QDs are highly oriented along the [0001] direction.

a)Author to whom correspondence should be addressed. Electronic mail: sbk@mrc.iisc.ernet.in.

 © 2011 American Institute of Physics

Downloaded 19 Sep 2013 to 142.51.1.212. This article is copyrighted as indicated in the abstract. Reuse of AIP content is subject to the terms at: http://jap.aip.org/about/rights_and_permissions

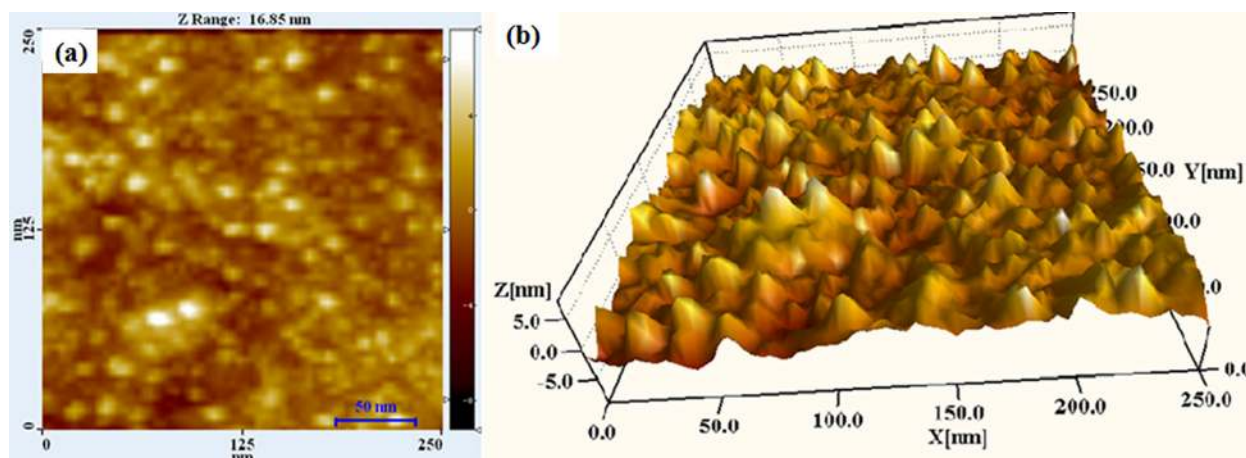

FIG. 2. (Color online) (a) STM image and (b) 3D STM images of InN QDs. The STM images were collected at room temperature under the tunneling current of 0.5 nA and sample bias −1.3 V.

chamber via the load-lock chamber. The Si substrate was thermally cleaned at 900 °C for several hours in ultrahigh vacuum. The deposition of InN consists of a two step growth method. The initial low temperature nucleation layer was deposited at 400 °C for 2 min. Further, the substrate temperature was raised to 500 °C to fabricate the QDS. The duration of QDs growth was kept for 30 min. The beam equivalent pressure, nitrogen flow rate, and plasma power were kept 1×10^{-7} mbar, 0.7 sccm, and 350 W. After growth, the samples of uncapped InN dots were transferred under UHV to the adjacent SPM chamber for surface characterizations. STS data and STM current mode images were collected using commercially available Pt-Ir tips. Constant current mode of STM was conducted at room temperature under the tunneling current of 0.5 nA and sample bias −1.3 V and STS was measured simultaneously on the top of individual dots applying −1.5 to 1.5 V. Topographic images of dots were collected by scanning simultaneously in the forward and backward directions together with constant current images, to insure that no distortion of the dot shape occurred due to tip effects. The structural and surface morphologies of these QDs were characterized by x-ray diffraction (XRD) and field emission transmission electron microscopy (TEM). The PL spectra were recorded at 10 K using a closed cycle optical cryostat and He-Cd laser of 325 nm excitation wavelength with a maximum input power of 30 mW.

III. RESULTS AND DISCUSSION

Structural characteristics of the as-grown InN QDs were evaluated by XRD. Figure 1 shows 2θ-ω scan of the InN QDs grown on Si (111) substrate. From the figure it can be seen that except the substrate peaks, only (0 0 0 2) InN diffracted peak at $2\theta = 31.35°$ is present, indicating the InN QDs to be highly oriented along the [0 0 0 1] direction of the wurtzite structures. Figures 2(a) and 2(b) show two-dimensional and three-dimensional (3D) STM images of InN QDs. The average size of InN QDs around ∼8 nm and density $\sim 6 \times 10^{11}$ cm^{-2} calculated from STM image. The STM images were collected at room temperature under the tunneling current of 0.5 nA and sample bias −1.3 V. Figure 3(a) represents typical bright field TEM micrograph of InN QDs, from which the size of the QDs was determined (∼8 nm). The corresponding high resolution TEM (HRTEM) image and selected area electron diffraction (SAED) of InN QDs are shown in Figs. 3(b) and 3(c). The HRTEM shows one of the corner edges of a QD and the interplanar spacing, as observed from the fringe pattern of the HRTEM image, is 0.305 nm, which corresponds to the (1 0 0 0) lattice spacing of InN.[18] The SAED pattern shows clearly visible bright spots which represents that each QD is single crystalline. These data clearly demonstrate that the as-grown QDs are fairly single crystalline, and are crystallized hexagonally

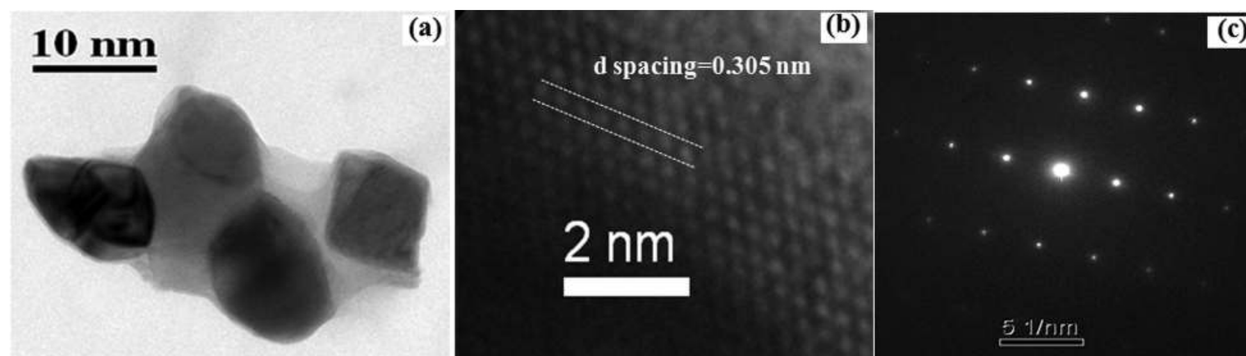

FIG. 3. (a) Typical TEM image of InN QDs. (b) HRTEM of InN QDs and the d spacing is measured 0.305 nm, which corresponds to the [1000] lattice spacing of InN. (c) Selected area electron diffraction (SAED) pattern was taken along the [0001] direction.

Downloaded 19 Sep 2013 to 142.51.1.212. This article is copyrighted as indicated in the abstract. Reuse of AIP content is subject to the terms at: http://jap.aip.org/about/rights_and_permissions

along the [0 0 0 1] direction with uniform geometry. The InN QDs were grown by two step growth, first low temperature nucleation layer at 400 °C and further high temperature growth at 500 °C. At higher growth temperature the surface mobility of In atoms are higher and according to the theory of surface growth, high mobility of In adatoms results randomly distributed dots of different sizes. We have adopted low-temperature "first-step" growth procedure, during which, the nucleation of dots likely completed.

The *I-V* curves were measured on different sizes of InN QDs using STS. Typical STM images of individual QDs and normalized conductance curves, $(dI/dV)/(I/V)-V$, are shown in Figs. 4(a) and 4(b). Diameters of these QDs are different as shown in figure but heights are almost same. Figures 5(a) and 5(b) show STM images of individual QDs and normalized conductance curves of almost same diameter (~7 nm) and different heights. In these profiles, the negative and positive tunneling current onsets represent the valence and conduction band edges, respectively.[19] A surface bandgap was found in the range 0.67 to 0.85 eV by measuring the difference between these tunneling onset voltages, and was found to be strongly dependent on the size of QD's. The

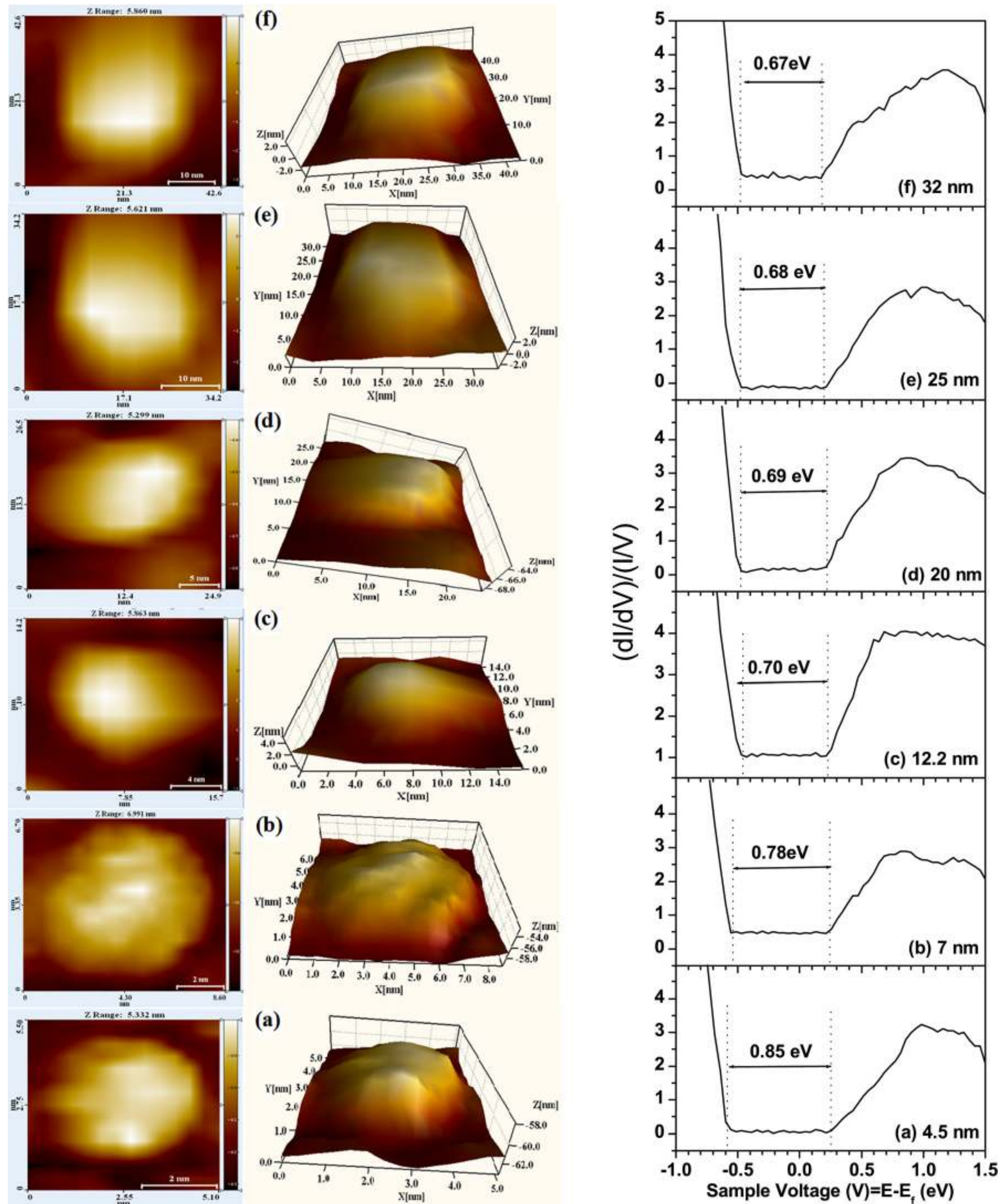

FIG. 4. (Color online) (a) STM images and (b) normalized conductance curves, $(dI/dV)/(I/V)-V$ of InN QDs of different sizes: (a) 4.5, (b) 7, (c) 12.2, (d) 20, (e) 25, and (f) 32 nm.

Downloaded 19 Sep 2013 to 142.51.1.212. This article is copyrighted as indicated in the abstract. Reuse of AIP content is subject to the terms at: http://jap.aip.org/about/rights_and_permissions

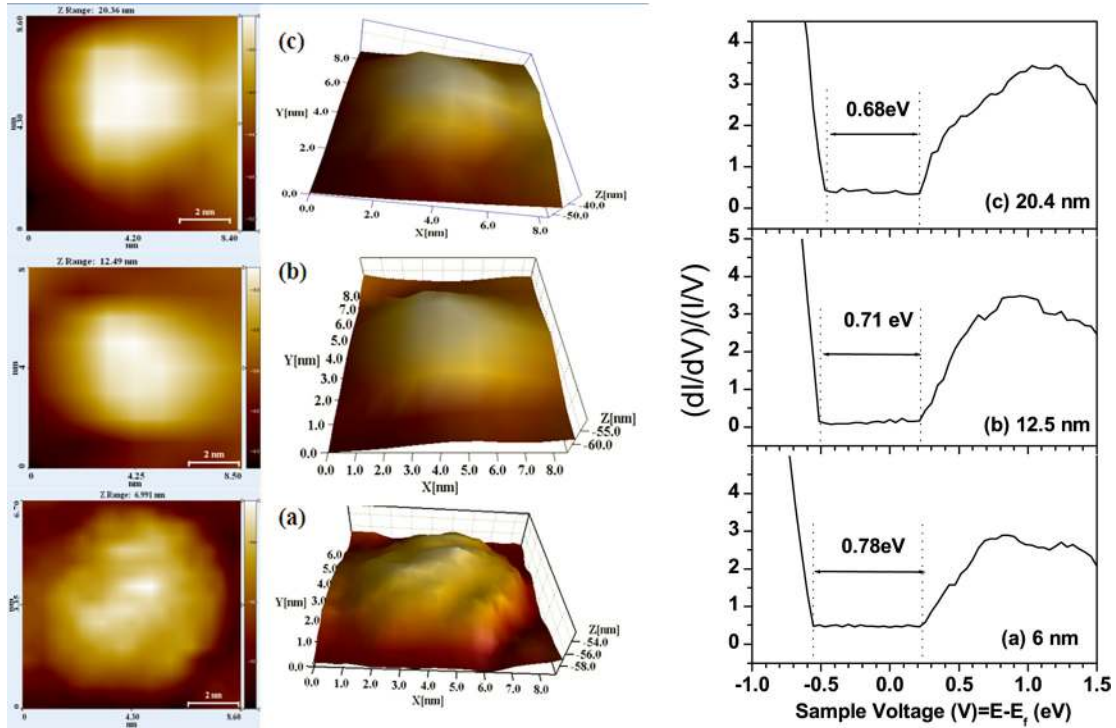

FIG. 5. (Color online) (a) STM images and (b) normalized conductance curves, $(dI/dV)/(I/V)-V$ of InN QDs of almost same diameter and different heights: (a) 6, (b) 12.5, and (c) 20.4 nm.

normalized conductance curves, $(dI/dV)/(I/V)-V$ curve in Figs. 4(b) and 5(b) exhibit neither intense peaks in the bandgap nor metallic properties. Thus, intrinsic surface states within the bandgap can be ruled out. An electron accumulation at the surface requires the Fermi level to be above E_C. However, in our case, E_F is pinned ~0.2 eV below E_C. Thus, accumulation current cannot arise from a charge carrier accumulation zone in the conduction band. Recently, Ebert *et al.* (Ref. 20) reported a further possibility is the tip-induced accumulation of electrons in the defect states pinning the Fermi level. These defect states lie directly at the Fermi energy and even a very small tip-induced band bending can induce a carrier accumulation in these states. However, the accumulation current and its $(dI/dV)/(I/V)$ signal are much smaller than those arising from the conduction and valence band states.

A theoretical estimation of the quantum size effect on a QD has been proposed by Nanda *et al.* (Ref. 21) based on a finite depth square well model and can be described by the following form:

$$\beta a \cot \beta a = 1 - \left(\frac{m^*}{m_0}\right) - \sqrt{\left(\frac{m^*}{m_0}\right)\left(\frac{V_0}{\Delta} - \beta^2 a^2\right)} \qquad (1)$$

with

$$\beta^2 = \frac{2m^*(E + V_0)}{\hbar^2} \quad \text{and} \quad \Delta = \frac{\hbar^2}{2m^* a^2}, \qquad (2)$$

where m^* stands for the effective mass of the electron or hole; the electron effective mass is 0.042 m_0,[22] and the hole effective mass is 0.1 m_0,[23] respectively. The diameter of the QD is $d = 2a$, and V_0 represents the confining potentials for electrons or holes. The electron confining potential is the electron affinity, which is 5.8 eV,[24] while it is 6.47 eV for the hole. The ground state transition between electrons and holes in a QD with radius a can be written as

$$E_g(a) = E_e(a) + E_h(a) + E_{e-h}(a) + E_g(bulk), \qquad (3)$$

where E_g(bulk) is the bandgap of bulk InN which is set to 0.67 eV in this work[25] and $E_{e\text{-}h}$ is coulomb energy. For the

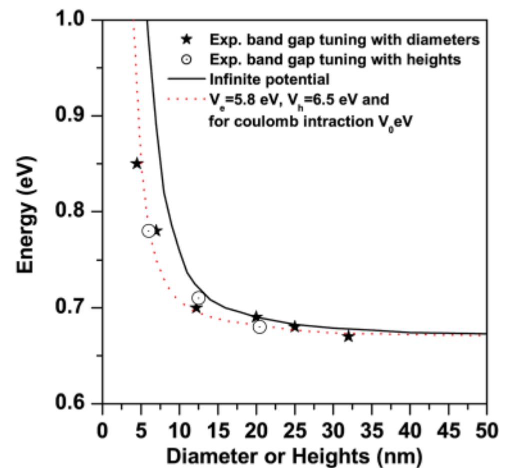

FIG. 6. (Color online) Calculated bandgap energy for InN QDs of various diameters and heights. The solid line represents the infinite potential theory, and the dotted line represents the electron and hole confining potential of 5.8 and 6.5 eV. The stars indicate experimental bandgap tuning with diameters and circles indicate experimental bandgap tuning with heights.

Downloaded 19 Sep 2013 to 142.51.1.212. This article is copyrighted as indicated in the abstract. Reuse of AIP content is subject to the terms at: http://jap.aip.org/about/rights_and_permissions

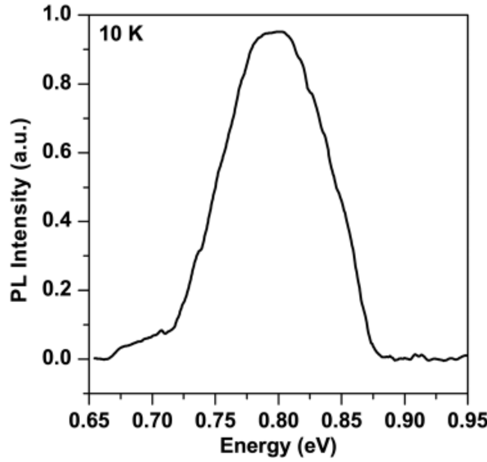

FIG. 7. Photoluminescence spectrum of InN QDs recorded at 10 K. The PL spectrum contained a broad peak around 0.80 eV.

coulomb interaction between an electron and a hole in a semiconductor is evaluated by

$$E_{e-h} = -\frac{16\pi^2 e^2 A_e^2 A_h^2}{\varepsilon a}\left[\int_0^a \sin^2(\beta_h r_h)dr_h - \frac{1}{2}\int_0^a \sin^2(\beta_h r_h)\sin(2\beta_e r_h)dr_h/r_h\right]. \quad (4)$$

For an infinite square-well potential ($V_0 \to$ infinite), the change in bandgap (ΔE_g) can be approximately written as

$$\Delta E_g(a) = \frac{\hbar^2\pi^2}{2a^2}\left(\frac{1}{m_e^*}+\frac{1}{m_h^*}\right) - \frac{1.75e^2}{4\pi\varepsilon\varepsilon_0 a}, \quad (5)$$

where m_e^* and m_h^* are the effective mass of electron and hole, respectively.

Figure 6 shows the calculated transition energy against the diameter and height of the QD. The experimental results are in good agreement with the theoretical calculations based on an EMA with finite-depth square-well potential model [Eq. (3)]. Experimental results do not follow the infinite potential well [Eq. (5)], which is also plotted in Fig. 6. The blueshift in the bandgap energy with the reduction in diameter and height of QD, is dominated by the quantum size effect.

The strain in the QDs could be another factor that affects the surface bandgap of InN QDs because it alters the electronic structures. In principle, the strain would tend to be higher in smaller sized QDs, since strain energy increases with volume thus prompting larger dots to relax. The bandgap would thus shift to higher energy due to the higher strain in smaller dots. The PL spectrum of the InN QDs measured at 10 K is shown in Fig. 7. Notably, the PL spectrum contained a broad peak around 0.80 eV which may be due to the presence of InN QDs with different sizes in the sample. The PL peak is blue shifted compared to the bulk InN, due to size dependent quantum confinement effect.

IV. CONCLUSION

In conclusion, InN QDs were grown on Si (111) by epitaxial Stranski-Krastanow growth mode using plasma-assisted MBE. Single-crystalline wurtzite structure of InN QDs was verified by the x-ray diffraction and TEM. A surface bandgap of InN QDs was estimated from STS *I-V* curves and found that it is strongly depend on the size of QDs. We observed a systematic blueshift in the bandgap energy as the QD's diameter or height was reduced. Theoretical calculations based on an effective mass approximation with finite-depth square-well potential model reveal the possibility that it is the quantum size effect that determines the observed size-dependent STS shifts.

[1]A. G. Bhuiyan, A. Hashimoto, and A. Yamamoto, J. Appl. Phys. **94**, 2779 (2003).
[2]J. Wu, W. Walukiewicz, K. M. Yu, J. W. Ager III, E. E. Haller, H. Lu, W. J. Schaff, Y. Saito, and Y. Nanishi, Appl. Phys. Lett. **80**, 3967 (2002).
[3]T. Matsuoka, H. Okamoto, M. Nakao, H. Harima, and E. Kurimoto, Appl. Phys.Lett. **81**, 1246 (2002).
[4]H. Lu, W. J. Schaff, J. Hwang, H. Wu, W. Yeo, A. Pharkya, and L. F. Eastman, Appl. Phys. Lett. **77**, 2548 (2000).
[5]T. Yamauchi, Y. Matsuba, L. Bolotov, M. Tabuchi, and A. Nakamura, Appl. Phys. Lett. **77**, 4368 (2000).
[6]V. D. Dasika, R. S. Goldman, J. D. Song, W. J. Choi, N. K. Cho, and J. I. Lee, J. Appl. Phys. **106**, 014315 (2009).
[7]S. Gaan, G. He, R. M. Feenstra, J. Walker, and E. Towe, Appl. Phys. Lett. **97**, 123110 (2010).
[8]L. E. Brus, J. Chem. Phys. **79**, 5566 (1983).
[9]K. K. Nanda, F. E. Kruis, and H. Fissan, J. Appl. Phys. **95**, 5035 (2004).
[10]S. V. Nair, L. M. Ramaniah, and K. C. Rustagi, Phys. Rev. B **45**, 5969 (1992).
[11]G. T. Einvoll, Phys. Rev. B **45**, 3410 (1992).
[12]N. A. Hill and K. B. Whaley, Phys. Rev. Lett. **75**, 1130 (1995).
[13]M. Lannoo, C. Delerue, and G. Allan, Phys. Rev. Lett. **74**, 3415 (1995).
[14]L. W. Wang and A. Zunger, Phys. Rev. B **53**, 9579 (1996).
[15]A. Franceschetti and A. Zunger, Phys. Rev. Lett. **78**, 915 (1997).
[16]A. Mizel and M. L. Cohen, Phys. Rev. B **56**, 6737 (1997).
[17]F. Buda, J. Kohanoff, and M. Parrinello, Phys. Rev. Lett. **69**, 1272 (1992).
[18]T. N. Bhat, B. Roul, M. K. Rajpalke, M. Kumar, S. B. Krupanidhi, and N. Sinha Appl. Phys. Lett. **97**, 202107 (2010).
[19]R. M. Feenstra, Phys. Rev. B **50**, 4561 (1994).
[20]P. Ebert, S. Schaafhausen, A. Lenz, A. Sabitova, L. Ivanova, M. Dähne, Y.-L. Hong, S. Gwo, and H. Eisele Appl. Phys. Lett. **98**, 062103 (2011).
[21]K. K. Nanda, F. E. Kruis, and H. Fissan, Nano Lett. **1**, 605 (2001).
[22]B. Arnaudov, T. Paskova, P. P. Paskov, B. Magnusson, E. Valcheva, B. Monemar, H. Lu, W. J. Schaff, H. Amano, and I. Akasaki, Phys. Rev. B **69**, 115216 (2004).
[23]W. C. Ke, C. P. Fu, C. Y. Chen, L. Lee, C. S. Ku, W. C. Chou, W. H. Chang, M. C. Lee, and W. K. Chen Appl. Phys. Lett. **88**, 191913 (2006).
[24]S. X. Li, K. M. Yu, J. Wu, R. E. Jones, W. Walukiewicz, J. W. Ager, W. Shan, E. E. Haller, H. Lu, and W. J. Schaff, Phys. Rev. B **71**, 161201(R) (2005).
[25]A. A. Klochikhin, V. Y. Davydov, V. V. Emtsev, A. V. Sakharov, V. A. Kapitonov, B. A. Andreev, H. Lu, and W. J. Schaff, Phys. Rev. B **71**, 195207 (2005).

Downloaded 19 Sep 2013 to 142.51.1.212. This article is copyrighted as indicated in the abstract. Reuse of AIP content is subject to the terms at: http://jap.aip.org/about/rights_and_permissions